Journal of Engineering Science and Technology
Vol. 17, No. 2 (2022) 1200 - 1212

SUPERSONIC STEAM EJECTORS: COMPARISON OF DRY AND WET-STEAM CFD SIMULATION MODELS

AHMED AL-MANEA[1,*]; KHALID SALEH[2]

[1]Al-Samawa Technical Institute, Al-Furat Al-Awsat Technical University, Iraq
[2]School of Mechanical Engineering, University of Southern Queensland, Australia
*Corresponding Author: Dr.ahmed.almanea@atu.edu.iq

Abstract

Ejectors are used widely in different vacuums applications. However, they still have low efficiency at the current time. Due to a lack of understanding of the ejector mixing process. This paper focuses on using Computational Fluid Dynamic (CFD) to understand the effect of condensation on the flow characterization after nozzle exit position. This was achieved by modelling a variable ejector geometry with two approaches: Ideal gas, and Wet-Steam models. The simulation outcome for both cases shows that the condensation process that occurs with the primary nozzle, led to a change in the static pressure and temperature magnitudes in comparison to the case without the condensation. The static temperature profile at NTP shows an increase within the static temperature in the Wet-Steam case with differences of approximately 180 K. In addition, the differences of static pressure after NTP for the two cases was approximately 1 K.

Keywords: CFD, Ideal gas model, Steam ejector; Supersonic flow, Wet-steam model.

1. Introduction

Ejectors or jets rely on high-speed mixing. An ejector is a pumping or compression device in which a higher pressure flow (called the primary flow) is used to induce a lower pressure-flow (called the secondary flow) into a mixing section. These two streams mix together and discharge to a pressure that lies between the initial pressures of these two fluids. The efficiency of the compression process depends in part, on the efficiency of the mixing between the two streams, and the deceleration of the mixed streams. An ejector typically consists of five main sections: (i) the primary inlet; (ii) the secondary inlet and suction chamber; (iii) the primary nozzle, (iv) the mixing chamber; and (v) the subsonic diffuser section, as illustrated in Fig. 1.

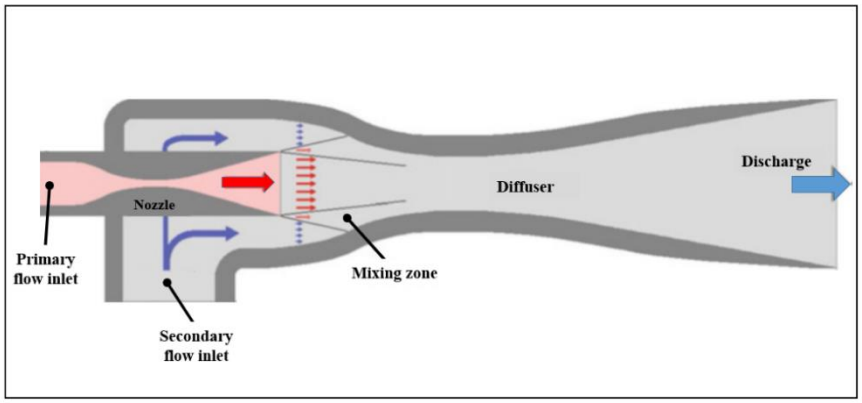

Fig. 1. General configuration of an ejector system [1].

In the case of steam ejectors, the mixing process is further complicated by the presence of condensation which introduces further uncertainties in the actual flow properties during mixing.

Over the past decades, significant work has been performed in the area of steam ejector studies, including experimental [2 – 4] and computational fluid dynamic (CFD) research [5]. These studies were focused on studying: the effect of the flow pattern, and operation conditions on ejector performance. In the CFD field, two approaches were used: Dry and Wet-Steam assumptions. Even though water vapour will tend to condense in the nozzle, the Ideal gas hypothesis has been used in many steam ejector CFD studies [3,6 – 9]. Within these studies, the main focus was to study the flow structure and to enhance the secondary flow mass to be entrained into the mixing chamber. Other studies have investigated the impact of vortices inside an ejector on the flow pattern [9].

The vapour expansion process in an ejector can be classified as either a dry vapour or a wet vapour, like steam [10]. Figure 2 shows the difference between the wet and dry vapour expansions. The saturated vapour line of the wet vapour case has a negative slope on the T-s diagram. The phase of the dry vapour is unchanged during the expansion process whereas small droplets are formed in the nozzle in the wet vapour case [11].

Although, this assumption requires less computational time for each CFD simulation [7], the effect of instant condensation inside the primary nozzle will not be taken into consideration for steam jet simulations. The Wet-Steam expansion

modelling approach is able to simulate the instant condensation with good agreement with experimental data whereas Ideal gas modeling cannot simulate this process [8].

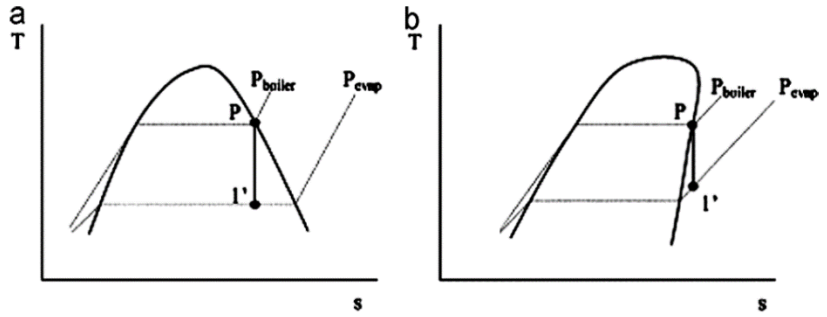

Fig. 2. T-s diagrams illustrating the expansion process through the nozzle: (a) Wet vapour, like steam; (b) Dry vapour, like some refrigerants [11].

This study is motivated by the need for a better understanding of flow properties downstream of the primary nozzle in a steam ejector. It also will provide more details on the effect of the condensation phenomenon on the mixing process. Thus, the present work seeks to investigate this effect by comparing two CFD models: (a) dry steam model (Ideal gas model); and (b) non-equilibrium model (Wet-Steam model).

2. Mathematical model

The phase of the dry vapour is unchanged during the expansion process whereas small droplets are formed in the nozzle in the wet vapour case [12].

The condensation phenomenon takes place instantly when the steam state exceeds the vapour-saturation line, due to a rapid expansion of the steam. Then this process leads the dry steam to initially subcool then nucleate to develop a mixture of saturated vapour and fine liquid droplets to form the wet steam. Therefore, the Wet-Steam consists of two phases, the first phase is the gaseous-phases which is the water-vapour, while the second phase is the liquid-phase consisting of condensed-water droplets.

As a step forward to investigate the condensation downstream of the nozzle, simulations in this paper have been performed using the multi-phase (Wet-Steam) model which is a two phase model integrated within ANSYS FLUENT. It solves the governing equations, with two other transport equations which are the liquid-phase mass fraction (β) and the number of the liquid droplets per unit volume (η). In ANSYS FLUENT, the following assumption is made within this model [13]:

- The interchange between droplets is ignored.
- The model has also limited the maximum liquid mass fraction (β) into a value no more than 0.2, due to the solution stability and converging problems.
- Droplet's volume is neglected, due to their tiny size (0.1 μm to 100 μm).
- Condensation is homogeneous.
- The model is unable to evaluate the ice formation within the low pressure region; as a result, it assumes the liquid temperature must always remain higher than 273 K which the triple point temperature.

The mixture density is associated to the vapour density,

$$\rho = \frac{\rho_v}{1-\beta} \tag{1}$$

Other mixture thermodynamic properties, such as the enthalpy, entropy, specific heat ratio among others are related to both of the liquid and vapour properties can be obtained by the following relationship [14] :

$$\phi_m = \phi_l\beta + (1-\beta)\phi_v \tag{1}$$

where ϕ is one of the mixture thermodynamic properties. The first additional transport equation to solve the condensation is the mass portion of the condensed liquid phase (β) [15]:

$$\frac{\partial\beta}{\partial t} + \nabla.(\rho\vec{v}\beta) = \Gamma \tag{2}$$

where Γ is the mass initiation rate due to the condensation and evaporation and it represents the sum of the accumulated mass due to nucleation and the growth of these droplets, and it can be presented as [15]:

$$\Gamma = \frac{4}{3}\pi\rho_l I r_*^3 + 4\pi\rho_l\eta\bar{r}^2\frac{\partial\bar{r}}{\partial t} \tag{4}$$

where r is the average radius of the droplet, and $r*$ is the critical radius of the droplet; higher than this value, the droplet will grow, and below and less than this value, evaporation will occur. The droplet critical radius is given by [16]:

$$r^* = \frac{2\sigma}{\rho_l RT \ln S} \tag{3}$$

where σ is the liquid surface tension, ρ_l is the density of the condensed liquid part, and S is the supersaturation ratio which is the ratio of vapour pressure to the equilibrium saturation pressure:

$$S = \frac{P}{P_{sat}(T)} \tag{4}$$

The condensation process is accomplished with two processes, the mass and heat transfer from the vapour to the droplets, this energy transference as the droplet growth rate (average radius change of the droplets), [15, 16]:

$$\frac{\partial\bar{r}}{\partial t} = \frac{P}{h_{lv}\rho_l\sqrt{2\pi RT}}\frac{\gamma+1}{2\gamma}C_p(T_o - T) \tag{7}$$

The other transport formula describes the growth of droplets number per unit volume of vapour, and it can be described as:

$$\frac{\partial(\rho\eta)}{\partial t} + \nabla.\left(\rho\vec{v}\eta\right) = \rho I \tag{8}$$

where η is the quantity of the number of the droplets per unit volume and can be represented as:

$$\eta = \frac{\beta}{(1-\beta)V_d\frac{\rho_l}{\rho_v}} \tag{9}$$

where V_d is the average volume of droplets. I is the nucleation rate. This has been described as a formation of the liquid as droplets of a supersaturated phase, and can be written as [11]:

$$I = \frac{q_c}{1+\theta}\left(\frac{\rho \upsilon^2}{\rho_l}\right)\sqrt{\frac{2\sigma}{M_m^3 \pi}} \exp\left(-\frac{4\pi r^{*2}\sigma}{3kT}\right) \quad (10)$$

The term q_c is the evaporation coefficient, M_m is the mass of one molecule, k is the Boltzmann constant (1.3807×10^{-23} J/K), σ is the liquid surface tension, and ρ_l represents the liquid density at the temperature T, and θ describes the non-isothermal correction factor is given by [16, 17]:

$$\theta = \frac{2(\gamma-1)}{\gamma+1}\frac{h_{lv}}{RT}\left(\frac{h_{lv}}{RT} - 0.5\right) \quad (11)$$

where h_{lv} is the specific enthalpy of evaporation at pressure P and the specific heat ratio γ. The equation of state which has been considered for the Wet-Steam in this work is given by [18]:

$$P = \rho_v R T_v . (1 + B\rho_v + C\rho_v^2) \quad (12)$$

where B and C are the second and third Virial coefficients. This equation can be used for either high and low pressures conditions within a range between (0.01-100) bar and temperature (273.15-1000) K [19].

3. Computational Simulation

The simulations within this section were carried out using two models; (1) Ideal gas; (2) Wet-Steam model. Within the Ideal gas model, the fluid was considered as an ideal gas, whereas Wet-Steam model the fluid domain was considered as real gas (steam).

3.1. Numerical solution method

The commercial CFD package ANSYS FLUENT *V* 19.1, was used to solve the governing equations numerically. A density-based, steady state (for Ideal gas), 2D axisymmetric solver, and realizable $k\omega-SST$ turbulent model with implicit formulations were used considering the accuracy and stability. A first-order upwind scheme was used for turbulent kinetic energy. The wall was set to have a stationary, non-slip condition. The convergence criteria used for the residual analysis was set to be 10^{-06} for continuity, X-velocity, Y-velocity, and Energy.

3.2. Model design and boundary conditions

The ejector and nozzle geometries that were used in this study correspond to the one presented in the previous study [20]. The shape and dimensions of this design are presented in Fig. 3, and Table 1.

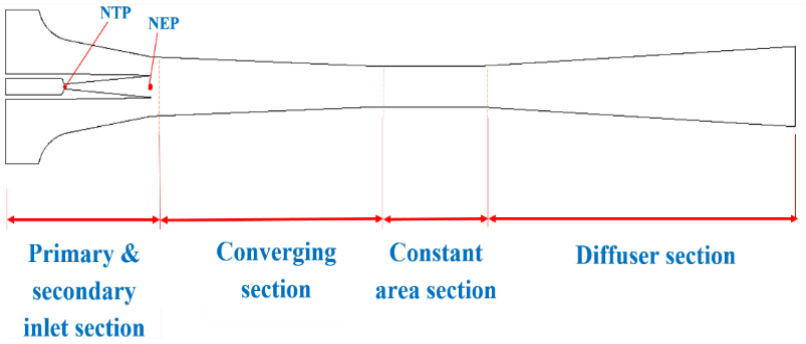

Fig. 3. Ejector 2D profile.

Table 1. Ejector design dimensions.

Component	Dimensions [mm]
Ejector overall length	551.7
Constant mixing area length	75
Nozzle length	101.5
Primary nozzle inlet diameter	10
Suction inlet diameter	96
Throat diameter	3.2
Constant mixing area diameter	25.5
Diffuser diameter	50

The boundary conditions were set for two inlets and one outlet in the ejector: The primary flow inlet, the suction flow inlet, and the outlet through the diffuser. Details about the boundary conditions used in CFD simulation are shown in Table 2.

Table 2. Nominal operating conditions.

	Pressure[kPa]	Temperature [K]
Primary stream	270	403
Secondary stream	1.6	287
Condenser	4.2	303

The mesh independence study was examined using three different grid sizes: A coarse mesh with 50,476 cells; a medium mesh with 80,802 cells; and a fine mesh with 115,87 cells, as shown in Fig. 4.

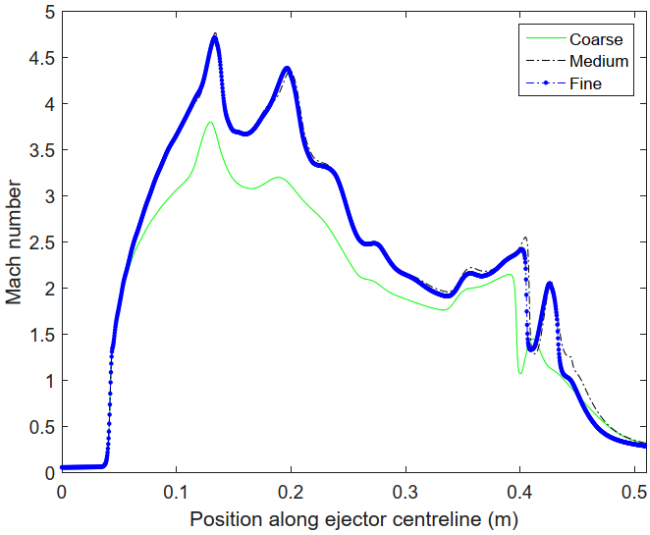

Fig. 4. Comparison of axial Mach number profiles for three mesh configurations.

Plots of the Mach number profile along the ejector's centreline show that results from the medium and the fine mesh are in good agreement with the difference in Mach number typically being less than 4%. However, larger differences between the region for positions > 0.4 m were noted. As a result, the medium mesh will be considered for simulations in this study.

4. Results and Discussions

4.1. Static pressure profile along the central axis

The static pressure profile for the ejector at the specified operating conditions is shown in Fig. 5. It is noted that there is a sudden pressure increase in Wet-Steam case in comparison to that of Ideal gas cases as condensation occurred.

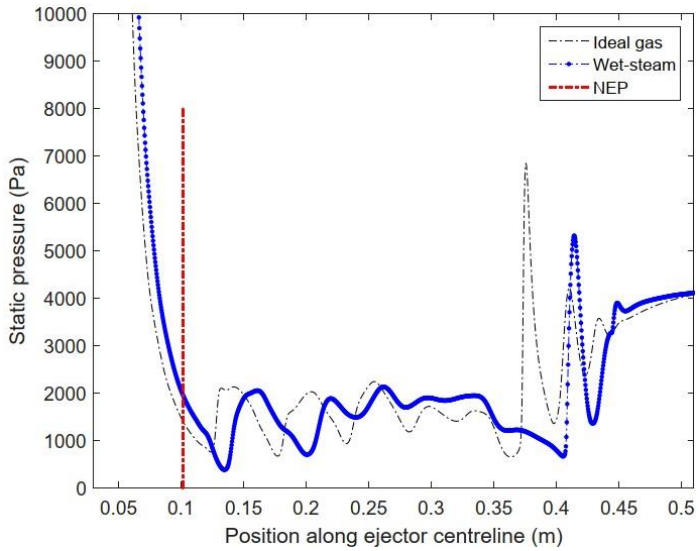

Fig. 5. Comparison of static pressure alone the ejector centreline for Ideal and Wet-Steam models, at P = 270 kPa, T = 403 K.

The flow after Nozzle Exit Position (NEP), shows fluctuation within static pressure along the centreline resulted from the series of diamond shock waves. At choke conditions of the ejector, a second set of oblique shock waves can be seen at the inlet section of the diffuser.

4.2. Mach number profile along the central axis

A comparison between Ideal gas and Wet-Steam cases has been made along the centreline of the primary nozzle. According to Fig. 5, Mach number profiles start to diverge just after Nozzle Throat Position (NTP). It is found also that there is a sudden descent of the Mach number of Wet-Steam to lower values than that observed for Ideal gas as condensation takes place. This difference arises from Wilson's point to the nozzle exit position as shown in Fig. 6.

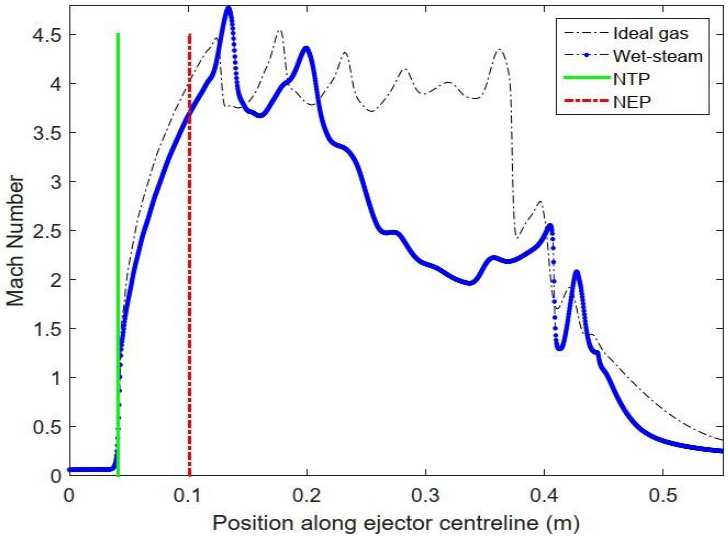

Fig. 6. Comparison Mach number profiles along ejector centreline for ideal and Wet-Steam models.

Additional comparison of contour plots for Mach number resulting from both model simulations is shown in Fig. 7.

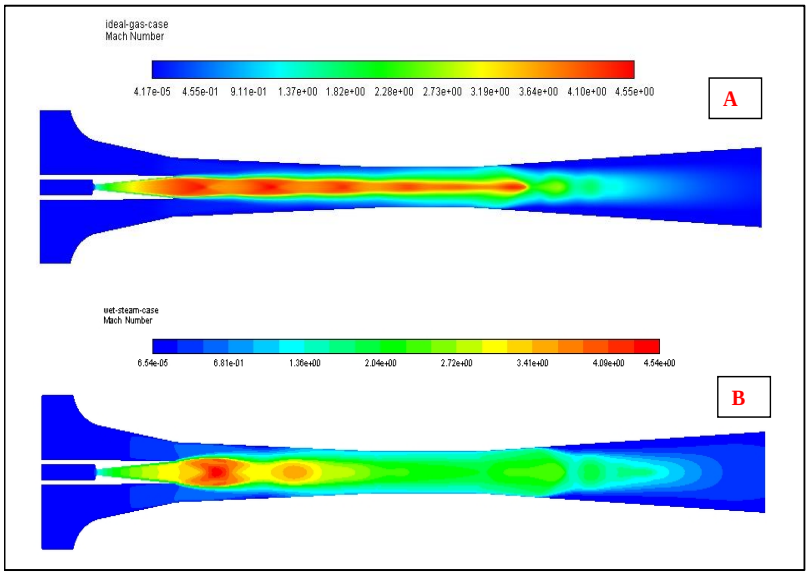

Fig. 7. Contour plot of Mach number profiles along ejector centreline (A) Ideal model; (B) Wet-steam model, at P = 270 kPa, T = 403 K.

4.3. Static temperature profile along the central axis

Figure 8 shows that there is a sudden increase associated with the temperature of Wet-Steam just after NTP, due to the large thermal-positive that resulted from spontaneous

condensation. The condensation temperature resulted from the growth of droplets that keep the Wet-Steam temperature much higher than that of a perfect gas.

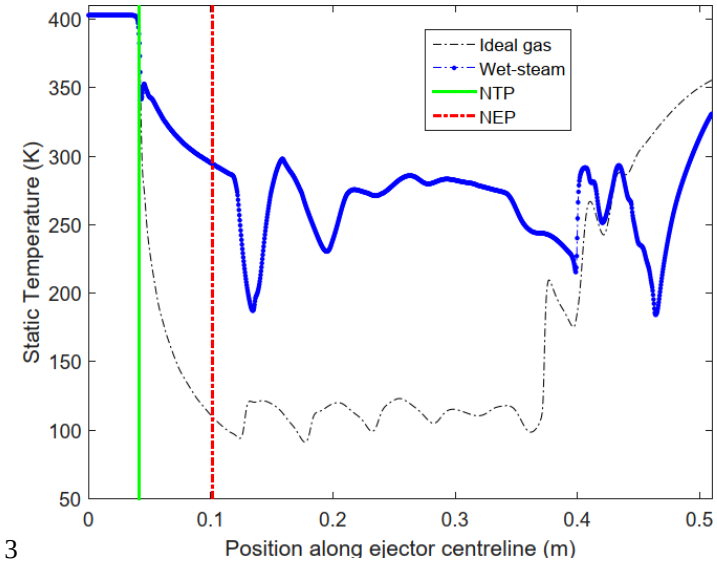

3

Fig. 8. Comparison of static temperature profiles along ejector centreline for Ideal and Wet-Steam models, at P = 270 kPa; T = 403 K.

4.4. Ejector nozzle's spontaneous condensation

Figures 9, 10, and 11 show spontaneous condensation characteristics inside the nozzle with Wet-Steam simulations. Figure 8 shows the saturation temperature of the vapour, which drops to around 260 K after NEP. The droplet nucleation rate and the droplet mass fraction grow rapidly after the nozzle's throat directly

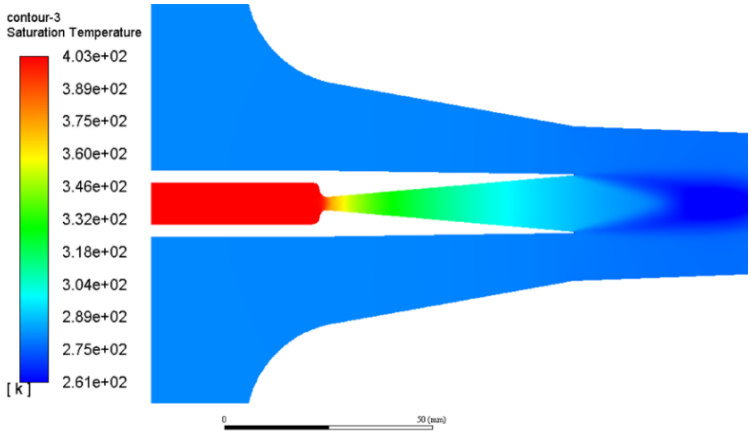

Fig. 9. Contour plot of saturation temperature of the vapour at P = 270 kPa, and T = 403 K.

This is happening due to a sudden drop in the pressure in this region.

The maximum mass fraction (wetness factor) as shown in Fig. 10, is less than 0.2 and this is well agreed with the assumption which has been considered to solve this model.

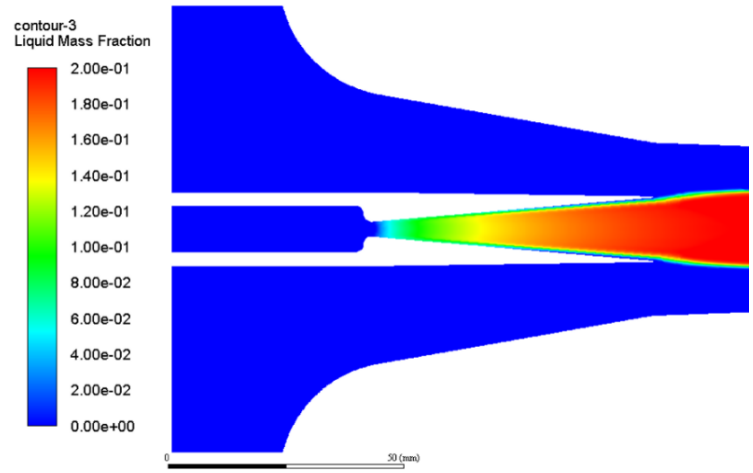

Fig. 10. Contour plot of liquid mass fraction at *P* = 270 kPa, and *T* = 403 K.

The droplet per unit volume refers to zero droplets that enter the nozzle prior to the expansion process. This value has rapidly increased through the expansion process within the nozzle's throat as shown within the droplet nucleation rate in Fig. 11.

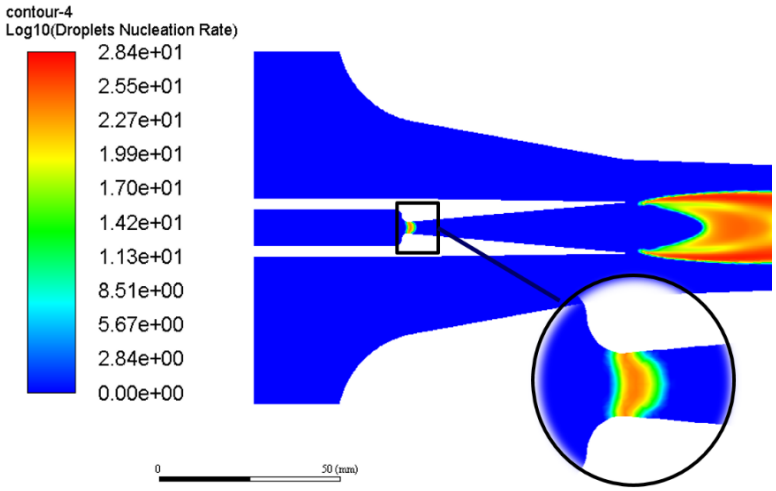

Fig. 11. Contour plot of droplet nucleation rate location at *P* = 270 kPa, and *T* = 403 K.

4.5. Validation of the numerical model

To validate numerical simulation results, a comparison to the literature was performed [21]. Figure 12 shows a comparison of the static pressure simulation results of the current study with previous work along the nozzle axis [21], with an average error of approximately 6 %. Additional comparison of simulation results of Mach number, with an average error of approximately 4%.

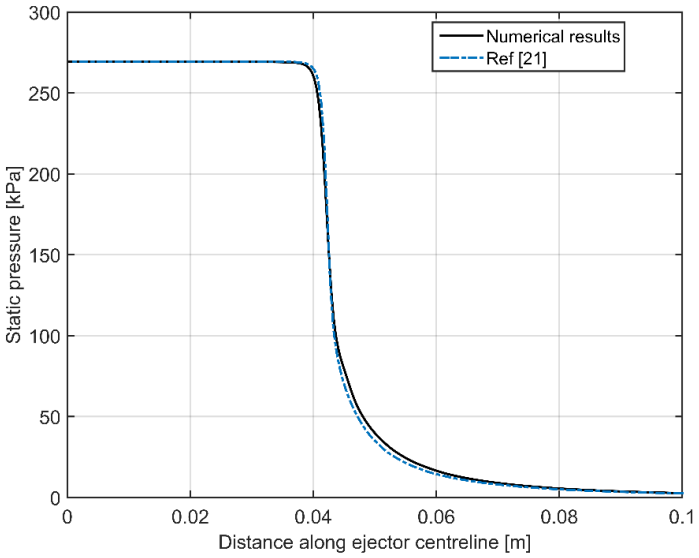

Fig. 12. Comparison of static pressure profiles along nozzle centreline, at P = 270 kPa; T = 403 K.

5. Conclusions

This paper has shown a comparison study between two different numerical approaches: Ideal gas, and Wet-Steam models, to understand the effect of the condensation that occurs with steam ejectors on flow behavior. The Wet-Steam model was successfully used to study the condensation inside the primary nozzle. The study concludes that due to the condensation process that occurs in the nozzle's throat. There was a change associated with both the static pressure and temperature. Comparison to the case without the condensation. The static temperature profile shows an increase within the static temperature with Wet-Steam case after (NTP) with differences of approximately 180 K. This is due to the heat that generates because of the condensation phenomenon. And, the difference of static pressure after (NTP) for the two cases was approximately 1 kPa.

6. Future work

For future work to improve the performance of steam jets, the condensation phenomenon can be studied within supersonic ejector to:

- Study its impact on the shear layer development between the primary and secondary steams inside an ejector.
- Study its impact within multi-phase flow streams.

Nomenclatures

h_{lv}	Specific enthalpy of vaporization, (J/kg).
I	Nucleation rate, (1/s m^3).
k	Boltzmann constant, (J/K).
M_m	Mass of one molecule
P	Pressure, Pa.
q_c	Evaporation coefficient.
r^*	Critical droplet radius, (m).
S	Super saturation ratio.
T	Temperature, K.
$\mathcal{R}$	Specific gas constant, (J/kg K).
T_o	Droplet temperature, (K).
V_d	Average droplet volume,(m^3)

Greek Symbols

Γ	Mass generation rate, (kg/m^3 s),
ρ_l	Condensed liquid density, (kg/m^3).
θ	Non-isothermal correction factor.
γ	Specific heat ratio.
σ	Liquid surface tension, (J/m^2).
β	liquid -phase mass fraction.
η	Number of the liquid droplets per unit volume, (1/m^3).

Abbreviations

CFD	Computational Fluid Dynamic.
NEP	Nozzle Exit Position.
NTP	Nozzle Throat Position.

References

1. Grazzini, G.; Milazzo, A.; and Mazzelli, F. (2018). *Ejectors for efficient refrigeration: design, applications and computational fluid dynamic.* Switzerland: Springer International Publishing.
2. Grazzini, G.; Milazzo, A.; and Paganini, D. (2012). Design of an ejector cycle refrigeration system. *Energy Conversion and Management*, 54(1), 38-46.
3. Al-Manea, A.; Buttsworth, D.R.; Leis, J.; and Saleh, K. (2019). Tunable diode laser absorption spectroscopy in a supersonic steam jet. *Proceedings of the 9th Australian Conference on Laser Diagnostics*. Adelaide, Australia, 91-94.
4. Al-Doori, G.; and Buttsworth, D.R. (2014). Pitot pressure measurements in a supersonic steam jet. *Experimental Thermal and Fluid Science*, 58(1), 56-61.
5. Ariafar, K.; Buttsworth, D.; Al-Doori, G.; and Sharifi, N. (2016). Mixing layer effects on the entrainment ratio in steam ejectors through ideal gas computational simulations. *Energy*, 95(1), 380-392.
6. Al-Manea, A.; Buttsworth, D.; Leis, J.; Choudhury, R.; and Saleh, K. (2018). Measurement of Water Vapour in Axisymmetric Jet Development Using TDLAS. *Proceedings of the 21st Australasian Fluid Mechanics Conference.* Adelaide, Australia, 10-13.

7. Kong, F.S.; Kim, H.D.; Jin, Y.Z.; and Setoguchi, T. (2012). Computational analysis of mixing guide vane effects on performance of the supersonic ejector-diffuser system. *Open Journal of Fluid Dynamics*, 2(3), 45-55.
8. Wang, X.; Dong, J.; Li, A.; Lei, H.; and Tu, J. (2014). Numerical study of primary steam superheating effects on steam ejector flow and its pumping performance. *Energy*, 78(20), 205-211.
9. Al-Manea, A.; and Al-Jadir, T. (2021). Effect of ejector design parameters on flow structure inside the mixing chamber. *IOP Conference Series: Earth and Environmental Science*, 779(1), 12-33.
10. Sih-Li, C.; Yen, J.-Y.; and Huang, M.-C. (1998). An experimental investigation of ejector performance based upon different refrigerants. *ASHRAE Transactions*, 104.
11. Varga, S.; Oliveira, A.C.; and Diaconu, B. (2009). Numerical assessment of steam ejector efficiencies using CFD. *International Journal of Refrigeration*, 32(12), 1203-1211.
12. Mazzelli, F.; Brezgin, D.; Murmanskii, I.; Zhelonkin, N.; and Milazzo, A. (2016). Condensation in supersonic steam ejectors: comparison of theoretical and numerical models. *Proceedings of the International Conference on Multiphase Flow.* Firenze, Italy.
13. ANSYS 2018 ANSYS-FLUENT 18.1 User's Guide.
14. Palma, M.G. (2014). *Numerical simulation of condensation in a supersonic nozzle for application to ejectors in refrigeration.* Master thesis, University of Catalonia, Belgium.
15. Ishizaka, K. (1995). A high-resolution numerical method for transonic non-equilibrium condensation flow through a steam turbine cascade. *Proceedings of the 6th International Symposium on Computational Fluid Dynamics.* Lake Tahoe, USA, 479-484.
16. Young, J.B. (1992). Two-dimensional, nonequilibrium, wet-steam calculations for nozzles and turbine cascades. *Journal of Turbomachinery*, 114(3), 569-579.
17. Gerber, A.G.; and Kermani, M.J. (2004). A pressure based Eulerian--Eulerian multi-phase model for non-equilibrium condensation in transonic steam flow. *International Journal of Heat and Mass Transfer*, 47, 2217-2231.
18. Young, J.B. (1988). An equation of state for steam for turbomachinery and other flow calculations. *Journal of Engineering for Gas Turbines and Power*, 110(1), 1-7.
19. Yang, Y.; and Shen, S. (2009). Numerical simulation on non-equilibrium spontaneous condensation in supersonic steam flow. *International Communications in Heat and Mass Transfer*, 36(9), 902-907.
20. Al-Doori, G.F.L. (2013). *Investigation of refrigeration system steam ejector performance through experiments and computational simulations*. PhD thesis, University of Southern Queensland, Australia.
21. Ariafar, K.; Buttsworth, D.; Sharifi, N.; and Malpress, R. (2014) Ejector primary nozzle steam condensation: Area ratio effects and mixing layer development. *Applied Thermal Engineering*, 71(1), 519-527.